

# Mrk 421 as a case study for TeV and X-ray variability in leptohadronic models

A. Mastichiadis (AM) <sup>\*</sup> M. Petropoulou (MP) <sup>†</sup> and S. Dimitrakoudis (SD) <sup>‡</sup>

*Department of Physics, University of Athens, Panepistimiopolis, GR 15783 Zografos, Greece*

Received.../Accepted...

## ABSTRACT

We investigate the origin of high-energy emission in blazars within the context of the leptohadronic one-zone model. We find that  $\gamma$ -ray emission can be attributed to synchrotron radiation either from protons or from secondary leptons produced via photohadronic processes. These possibilities imply differences not only in the spectral energy distribution (SED) but also in the variability signatures, especially in the X- and  $\gamma$ -ray regime. Thus, the temporal behavior of each leptohadronic scenario can be used to probe the particle population responsible for the high-energy emission as it can give extra information not available by spectral fits. In the present work we apply these ideas to the non-thermal emission of Mrk 421, which is one of the best monitored TeV blazars. We focus on the observations of March 2001, since during that period Mrk 421 showed multiple flares that have been observed in detail both in X-rays and  $\gamma$ -rays. First, we obtain pre-flaring fits to the SED using the different types of leptohadronic scenarios. Then, we introduce random-walk type, small-amplitude variations on the injection compactness or on the maximum energy of radiating particles and follow the subsequent response of the radiated photon spectrum. For each leptohadronic scenario, we calculate the X-ray and  $\gamma$ -ray fluxes and investigate their possible correlation. Whenever the ‘input’ variations lead, apart from flux variability, also to spectral variability, we present the resulting relations between the spectral index and the flux, both in X-rays and  $\gamma$ -rays. We find that proton synchrotron models are favoured energetically but require fine tuning between electron and proton parameters to reproduce the observed quadratic behaviour between X-rays and TeV  $\gamma$ -rays. On the other hand, models based on pion-decay can reproduce this behaviour in a much more natural way.

**Key words:** astroparticle physics – radiation mechanisms: non-thermal – gamma rays: galaxies – galaxies: active – BL Lacertae objects: general

## 1 INTRODUCTION

Blazars are a subclass of Active Galactic Nuclei (AGN) with a non-thermal emission covering most of the electromagnetic spectrum, i.e. from radio up to high-energy gamma-rays. Their broadband emission, that originates from a relativistic jet oriented close to the line of sight, is Doppler boosted and shows no evidence of spectral lines. The spectral energy distribution (SED) of TeV-emitting blazars consists of two smooth, broad components (e.g. Ulrich et al. 1997; Fossati et al. 1998). The first one extends from the radio up to the X-rays with a peak in the soft or hard X-rays, while the second one extends up to TeV energies, with a peak

energy around 0.1 TeV, although this is not always clear (Abdo et al. 2011).

Although the lower energy bump is attributed to the synchrotron radiation of relativistic electrons, the origin of the high-energy component is still under debate. Theoretical models are divided into two classes: (i) leptonic and (ii) (lepto)hadronic, according to the type of particle responsible for the  $\gamma$ -ray emission. In the leptonic scenario, the high-energy component is the result of Compton scattering of electrons on a photon field; the seed photons can come either from synchrotron emission of the same electron population (SSC models) (e.g. Maraschi et al. 1992; Konopelko et al. 2003) or from an ‘external’ region, i.e. from the accretion disk (Dermer et al. 1992; Dermer & Schlickeiser 1993) or from the broad line region (Sikora et al. 1994; Ghisellini & Madau 1996; Boettcher & Dermer 1998) (EC models). In the hadronic scenario, on the other hand,

<sup>\*</sup> E-mail: amastich@phys.uoa.gr

<sup>†</sup> E-mail: maroulaaki@gmail.com

<sup>‡</sup> E-mail: sdimis@phys.uoa.gr

the  $\gamma$ -ray emission is the result of proton or secondary lepton (through photohadronic interactions) synchrotron radiation (Mannheim & Biermann 1992; Aharonian 2000; Mücke et al. 2003). For a recent review see Boettcher (2012).

The above models have been successfully applied for fitting the overall SED of TeV blazars by assuming stationary conditions, at least in most cases – this is particularly true for the class of hadronic models. However, one major feature of blazar emission is the variability observed in almost all energies (see for example Raiteri et al. 2012), which further implies that stationary conditions might not apply. Moreover, variability can provide additional constraints on source modelling and therefore it can be used to lift the apparent degeneracy between leptonic and hadronic models. As the above models use very different processes of widely varying cooling timescales, one expects that the system will react in a different way to variations on one or more source parameters, such as the injection rate of fresh particles. For example, one of the successes of SSC leptonic modelling is that it can reproduce the quadratic behaviour between the X-ray and TeV fluxes (Mastichiadis & Kirk 1997; Krawczynski et al. 2002). The lack, thus far, of time-dependent hadronic models, has forbidden an analogous study of their expected radiative signatures.

Recently Dimitrakoudis et al. (2012) have presented an one-zone hadronic model which is time-dependent. In the present paper we make use of the numerical code presented there in search for variability signatures in the context of these models. As an illustrative example, we have chosen to focus on the relatively recent, high quality observations of Mrk421 Fossati et al. (2008), that provide us with both spectral and temporal information. While we do not attempt to make a detailed spectral or temporal fit to the observations, we use these as a springboard to examine the trends expected within the hadronic models.

The present paper is organized as follows: In §2 we present the basic principles of the one-zone hadronic model and we comment on the possible options for fitting the SED of a blazar; the type of variations adopted in our simulations is also presented. In §3 we present our results starting with the multiwavelength (MW) fits obtained using three different (lepto)hadronic models. In subsections 3.2 - 3.3 we present the variability signatures obtained for each model caused by variations that we have applied on the injection compactness or on the maximum energy of particles respectively. We conclude in §4 with a summary and a discussion of our results. For the required transformations between the reference systems of the blazar and the observer, we have adopted a cosmology with  $\Omega_m = 0.3$ ,  $\Omega_\Lambda = 0.7$  and  $H_0 = 70$  km s<sup>-1</sup> Mpc<sup>-1</sup>, where the redshift of Mrk 421  $z = 0.031$  corresponds to a luminosity distance  $D_L = 0.135$  Gpc.

## 2 THE MODEL

### 2.1 General Principles

In what follows we use the one-zone hadronic model as described in Dimitrakoudis et al. (2012) – henceforth DMPR. For completeness reasons we repeat here its basic points. We consider a spherical blob of radius  $R$  moving with a Doppler factor  $\delta$  with respect to us and containing a magnetic field

of strength  $B$ . We further assume that ultra-relativistic protons with a power law distribution of index  $p_p$  between some energy limits  $\gamma_{p,\min}$  and  $\gamma_{p,\max}$  are injected into the source (we will be using Lorentz factors to denote proton or electron energies throughout this paper). This injection can be characterised by a compactness

$$\ell_p^{\text{inj}} = \frac{L_p \sigma_T}{4\pi R m_p c^3} \quad (1)$$

where  $L_p$  is the proton injected luminosity and  $\sigma_T$  is the Thomson cross section.

Protons can lose energy via three channels: (a) synchrotron radiation, (b) photopair (Bethe-Heitler) and (c) photopion production. The effect that any of those three processes has on the proton distribution function depends on the specific parameters of the system, therefore all three have to be taken into account in a kinetic equation that also includes a proton injection and a proton escape term. Furthermore, since the above processes will create photons and other secondary particles (which will eventually decay to electrons and positrons, both of which we will hereafter refer to as electrons), one has to also follow the evolution of photons and electrons, by writing two additional kinetic equations for them<sup>1</sup>. Assuming that the particles have a uniform distribution inside the source, one can write a system of partial, with respect to time and energy, integrodifferential equations, whose solution gives the corresponding particle distribution in addition to the multiwavelength photon spectrum emerging from the source.

The total number of free parameters used in this case is eight: The radius  $R$  of the source, the magnetic field strength  $B$ , the proton injection compactness  $\ell_p^{\text{inj}}$ , the lower and upper Lorentz factors of the proton power law distribution  $\gamma_{p,\min}$  and  $\gamma_{p,\max}$ , as well as the proton index  $p_p$  and the escape time from the source  $t_{p,\text{esc}}$ . To these one should add the Doppler factor  $\delta$  of the emitting blob, which is used to boost the radiation and convert the source-frame quantities into observed flux.

In the case where electrons are injected, in addition to protons, one could introduce the corresponding electron parameters which are their injection compactness  $\ell_e^{\text{inj}}$ , which is related to their luminosity  $L_e$  in the same way as described in eq. (1) with  $m_e$  replacing  $m_p$ , the upper and lower cut-off of their injected spectrum  $\gamma_{e,\min}$  and  $\gamma_{e,\max}$  respectively, their slope  $p_e$  and their escape timescale  $t_{e,\text{esc}}$ . In order to reduce the number of free parameters one can assume that  $\gamma_{p,\min} = \gamma_{e,\min} = 1$  and  $t_{p,\text{esc}} = t_{e,\text{esc}}$ .

Depending on the assumptions made about the time dependence of the parameters, the above scheme can be used to derive both steady-state and time-dependent solutions. Thus, if all parameters are constant in time the system will eventually reach a steady-state – note however that hadronic plasmas can become supercritical and in such cases they can exhibit limit cycle behaviour (Petropoulou & Mastichiadis 2012b) – hereafter PM12b. If, on the other hand, the system is in the subcritical regime and we allow for one or more parameters to have some explicit time dependence, then the

<sup>1</sup> Neutrons and neutrinos are also byproducts of photopionic interactions and one therefore should, in principle, write two more equations for them – see DMPR. For our present case, however, one can safely ignore them.

system will not reach a steady state but it will show continuous temporal variations, which will reflect the corresponding ones imposed on the input parameters and will have an impact on the produced spectrum.

Therefore, one can first use the numerical code to obtain the SED of a source in a stationary state and then introduce perturbations in one or more of the fitting parameters to check the variability patterns in the MW spectrum. Similar methods have been applied in the case of leptonic models by Mastichiadis & Kirk (1997) and Krawczynski et al. (2002). However, in the framework of hadronic modelling we find that there are different combinations of radiative processes which can, in principle, give acceptable fits to the SED of blazars. Thus, it is possible that each fitting combination will have distinct temporal signatures which are worth investigating. In what follows we make a qualitative discussion on the various options one has of fitting the SED of blazars using a hadronic model and then present our method regarding temporal variations.

## 2.2 Fitting the SED

In contrast to the leptonic model where the relevant radiative processes are few, the hadronic model involves many processes which can make the radiated spectrum quite complicated. However, as it was shown in DMPR, there are certain limiting, yet intuitive, cases, where the derived spectrum has a particularly simple form. Thus, in the case where all features in the MW spectrum can be attributed to protons<sup>2</sup>, a case we will refer to as ‘pure hadronic’ or simply ‘model H’, the spectrum has four distinctive features. One due to proton synchrotron radiation, two due to synchrotron radiation of electrons produced respectively in photopair and charged pion decay and one due to  $\gamma$ -rays from neutral pion decay. What is also interesting is that the frequencies where the three first peaks occur have a fixed ratio between them and scale as  $(m_e/m_p) : 1 : \eta_{pe}^2$  where the value  $\eta_{pe} \simeq 150$  is deduced empirically from the results of the SOPHIA code (Mücke et al. 2000). So the frequencies of the first and third peaks are about eight orders of magnitude apart and therefore if the first one happens to be in the X-ray regime then, interestingly enough, the third one will be at TeV  $\gamma$ -rays<sup>3</sup>. Clearly this coincidence needs some investigation as far as MW modelling is concerned.

The introduction of a high luminosity leptonic component can change the picture significantly. If electrons have suitable parameters as to explain the X-rays, then there are two different options for fitting the TeV  $\gamma$ -rays with protons. The first is from the process described above, i.e.  $\gamma$ -rays are produced from a combination of the synchrotron radiation of electrons produced in charged pion decay and of the electromagnetic cascade induced from neutral pion decay. We shall refer to this mechanism for TeV  $\gamma$ -ray production as ‘pion induced’ and we will denote the model with the acronym

‘LH $\pi$ ’. As it turns out this model requires proton Lorentz factors not higher than  $10^7$  and intermediate magnetic field strengths ( $\sim 10$  G). The same holds, in general, for model H.

The second option is to fit the SED with very high proton energies ( $\gamma_{p,\max} \sim 10^{10}$ ) and high magnetic fields ( $> 20$  G). In the latter case, proton synchrotron emission is responsible for the TeV emission – this is the most popular fitting method of the relevant observations and we will refer to it as the ‘proton-synchrotron’ case or as ‘LHs model’. Finally, both LH $\pi$  and LHs models fall into the more general category of ‘lepto-hadronic’ cases.

The above picture holds for low enough compactnesses. For higher ones photon-photon absorption, especially of the  $\pi^0$ -component that always peaks at very high frequencies, begins to dominate. However, as it was discussed in PM12b, the absorbed energy will be reemitted mostly at frequencies close to the peak produced by the radiation of charged pion-produced electrons, and only if the compactness becomes relatively high will the photon-photon absorption process become severe enough to distort the spectrum through electromagnetic cascades and redistribution to lower frequencies. At still higher compactnesses the system undergoes a phase-transition and it becomes supercritical: various radiative loops such as photopair-synchrotron (Kirk & Mastichiadis 1992) and photon quenching (Stawarz & Kirk 2007; Petropoulou & Mastichiadis 2011) rapidly take energy away from the protons and redistribute it to electrons and radiation. In this case the system becomes very efficient, since a large fraction of the input proton luminosity is turned into radiation; however this is done at the cost of the spectral features described earlier which are destroyed by a very strong, non-linear photon-photon absorption. Clearly one should seek successful spectral fits of MW blazar observations while the system is in the subcritical regime; note however that one can use supercriticalities in various contexts (Mastichiadis & Kazanas 2006, 2009; Petropoulou & Mastichiadis 2012a).

## 2.3 An algorithm for inducing time variability

DMPR have examined some examples of variability in the case of a pure hadronic model and showed that the system behaves like a SSC leptonic one, in the sense that proton synchrotron radiation produces the soft photons which act as targets for the photopair and photopion processes. Thus, in complete analogy to the leptonic SSC, hadrons interact with their own radiation. Consequently, one expects that variations in the proton injection parameter will produce a quadratic relation between the proton synchrotron and the pion induced components.

While the inclusion of primary electrons introduces more free parameters in the model and facilitates the spectral fitting, it complicates the problem of inducing variability since now one should introduce two more free parameters, one of which relates the amplitude of variations between electrons and protons while the other relates their phases. In other words, while the pure hadronic model is expected to have a well-predicted temporal behaviour, since variations can be induced by changing a single parameter, the lepto-hadronic models will have, by necessity, more complicated temporal patterns.

<sup>2</sup> A primary leptonic component may also exist, provided its contribution to the synchrotron emission is much smaller than that of protons – see Appendix A for more details.

<sup>3</sup> Note that, as pointed by PM12b, the electromagnetic cascade that ensues from the absorption of the  $\pi^0$ -decay  $\gamma$ -rays also contribute to the same energy regime.

In order to simulate temporal variations we will adopt the following algorithm:

(i) First we will obtain fits to a stationary/low state SED of a TeV blazar with each of the three aforementioned models (H,  $\text{LH}\pi$ , LHs).

(ii) We will then introduce variations on some key parameter (injection luminosity or maximum energy of particles) and follow in time the changes that these perturbations introduce to the SED of the source.

(iii) Since most observations focus on the correlation between X-rays and TeV  $\gamma$ -rays, we will focus on these energy bands and find the correlations expected in each of these three different scenarios.

For concreteness, we will apply this approach to the observations of Mrk 421 by Fossati et al. (2008). These sessions have produced a wealth of good quality, time-dependent data both at the X-ray (*RXTE*) and TeV (H.E.S.S.) regimes. However, we should warn the reader that we do not use the above data in order to make detailed fits but rather as a basis for comparing the general trends of our simulations with respect to them. Specifically, in the first step of the algorithm described above, we do not attempt a very detailed fitting of the SED but we use the approach of Petropoulou & Mastichiadis (2012a), where a family of possible fits with low reduced  $\chi^2$  (below 1.5) can be considered as acceptable.<sup>4</sup> At any rate, it turns out that the expected temporal variations presented in §3 are largely independent of the value of the  $\chi^2$  of the particular fit.

Motivated by the results of long-term variability studies of Mrk 421 and other prototype blazars (e.g. Emmanoulopoulos et al. (2010)), we have introduced, for the temporal variations, a random-walk type of change in one of the fitting parameters. Thus, we use

$$a_{i+1} = a_i + (-1)^{\text{int}(\xi)}, \quad i = 0, 1, 2, \dots \quad (2)$$

where  $\xi$  is a uniformly distributed random number in the range (0,10). The integer parameter  $a_i$  is then scaled in such a way as to produce the following change in the parameter  $y$  we wish to vary

$$y_i = y_0(1 + f a_i), \quad i = 1, 2, \dots \quad (3)$$

where  $y_i$  is the value of the parameter at time  $t_i$  and  $f$  a multiplication factor – in all the examples shown in the present paper we have chosen  $f = 0.05$ , i.e. the parameter in question varies only by 5% between crossing times. For the values of  $y$  between two successive crossing times, we have chosen a linear interpolation scheme. Obviously  $a_0 = 0$ , in order for the initial value of the parameter in question to match its corresponding value in the steady state fit  $y_0$ .

### 3 RESULTS

We proceed next to show some characteristic results. We will begin by showing the spectral fits obtained and then we will focus on the variability induced on the models by varying

<sup>4</sup> Clearly introducing more free parameters would have improved the fit but this would have acted against the scope of the present paper.

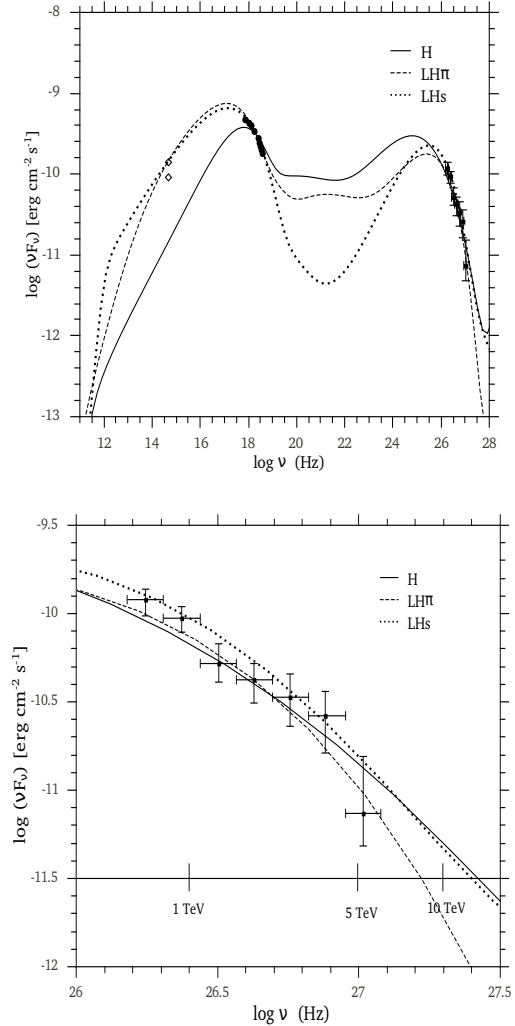


**Figure 1.** Top panel: Multiwavelength fit to the March 22nd/23rd data of Mrk 421 using (a) a purely hadronic one-zone model (solid line), (b) a leptohadronic one-zone model where the TeV component of the SED is produced by synchrotron radiation of electrons resulting from photohadronic interactions (dashed line), and (c) as before but with the TeV component of the SED produced by proton synchrotron radiation (dotted line). For the parameter used see Table 1. Bottom panel: The above zoomed in on the TeV energy range.

first the injection compactness ( $\ell^{\text{inj}}$ ) and then the maximum energy ( $\gamma^{\text{max}}$ ) of particles.

#### 3.1 Spectral fits

Figure 1 (top panel) shows the spectral fits we obtained using the three models described in the previous section to the pre-flaring state of Mrk 421 on the night of 22nd/23rd March 2001. All data points used for the fitting are contemporaneous; for more details on the observations see Fossati et al. (2008). Different types of lines correspond to different models as shown in the plot. A zoom in the TeV energy range is also shown in the bottom panel of the same figure. Note that, in all three models, the TeV  $\gamma$ -rays are fitted with the cutoff of the proton (LHs) or secondary lepton (H,  $\text{LH}\pi$ )

**Table 1.** Parameters for the pure hadronic and lepto-hadronic fits to the pre-flaring state of Mrk 421 (see Fig. 1).

Parameter symbol	Model H	Model LH $\pi$	Model LHs
$R$ (cm)	$3.2 \times 10^{15}$	$3.2 \times 10^{15}$	$3.2 \times 10^{15}$
$B$ (G)	20	5	50
$u_B$ (erg cm $^{-3}$ )	15.9	1.0	99.5
$\delta$	16	31	21
$t_{\text{var}}^{\text{obs}}$ (hr)	1.8	0.9	1.4
$\gamma_{p,\text{max}}$	$8 \times 10^5$	$4 \times 10^6$	$4 \times 10^9$
$p_p$	1.3	1.5	1.5
$\ell_p^{\text{inj}}$	$1.6 \times 10^{-2}$	$7.9 \times 10^{-4}$	$1.6 \times 10^{-7}$
$\gamma_{e,\text{max}}$	–	$3 \times 10^4$	$8 \times 10^3$
$p_e$	–	0.7	0.5
$\ell_e^{\text{inj}}$	–	$2 \times 10^{-5}$	$5 \times 10^{-5}$
$u_p$ (erg cm $^{-3}$ ) <sup>1</sup>	$3.2 \times 10^4$	$1.6 \times 10^3$	$2.9 \times 10^{-1}$
$u_e$ (erg cm $^{-3}$ )	$2.3 \times 10^{-4}$	$2 \times 10^{-3}$	$3.4 \times 10^{-3}$
$u_\gamma$ (erg cm $^{-3}$ )	1.2	0.1	$3.6 \times 10^{-1}$
$P_{\text{jet}}^{\text{obs}}$ (erg/s)	$6.9 \times 10^{48}$	$1.3 \times 10^{48}$	$2.4 \times 10^{44}$

<sup>1</sup> The listed particle and photon energy densities correspond to the pre-flaring fit, i.e. to a steady state of the system.

synchrotron spectrum; in the latter cases (H and LH $\pi$ ), synchrotron radiation from Bethe-Heitler electrons produce a distinctive broad spectral feature which lies between the proton synchrotron and the pion induced components. The fitting parameters of each model are listed in Table 1. In addition, the comoving energy densities of protons ( $u_p$ ), electrons ( $u_e$ ) and photons ( $u_\gamma$ ) at the steady state are listed. The observed luminosity of the jet has been calculated according to

$$P_{\text{jet}}^{\text{obs}} \approx \pi R^2 \delta^2 \beta c (u_B + u_p + u_e + u_\gamma). \quad (4)$$

Although all three models can give us acceptable fits to the SED, the pure hadronic is the most energy demanding, having the largest ratio of particle to magnetic energy density ( $u_p/u_B \approx 2 \times 10^3$ ) and the highest jet luminosity. Clearly, as far as energy requirements go, the proton synchrotron model is, by far, the most economic of the three.

### 3.2 Varying $\ell_p^{\text{inj}}$

One straightforward way of producing flaring activity is to vary the injection luminosity of the high-energy radiating particles. Thus, we start with the pure hadronic case and choose the proton injected compactness  $\ell_p^{\text{inj}}$  to be the varying parameter. Top panel of Fig. 2 depicts the X-ray (middle) and the TeV lightcurves (bottom) centered at  $10^{18}$  and  $2.5 \times 10^{26}$  Hz respectively. We note that, in what follows, any reference to the TeV and X-ray fluxes will mean the integrated fluxes in the ranges  $(1.6 \times 10^{26} - 10^{27})$  Hz and  $(7.2 \times 10^{17} - 3.6 \times 10^{18})$  Hz respectively. For comparison reasons, the injected proton luminosity (top curve) is also plotted after being rescaled.

In the bottom panel of the same figure, the power spectral densities (PSD) of the injection and TeV light curves are shown with black and grey lines respectively. The corresponding PSD for the X-ray light curve is not shown, since

it is similar to that of the TeVs apart from a normalization factor. While the PSD of the injection time-series can be fitted by a power-law with slope  $\sim -1.9$ , in agreement with the characteristic  $-2$  slope of brownian noise, the PSD of the TeV light curve is best fitted with a broken power-law having the same slope with the injection's PSD at low frequencies (large timescales) but steepens significantly at higher frequencies ( $f \gtrsim 0.1$ ). We note that same behaviour has been also detected in the two lepto-hadronic models. A study of the fitting parameters reveals that for protons producing the TeV  $\gamma$ -rays the condition  $t_{\text{cool}} \gg t_{\text{esc}} = t_{\text{cr}}$  holds, thus the system responds fast to the imposed variations due to the small value of the proton escape time. On the other hand, electrons radiating in the X-rays have a much faster cooling than escape timescale. However, their PSD produces also a break at about the same frequency as in the TeV  $\gamma$ -rays case. This behaviour seems puzzling at first; one would expect that if the cooling of particles is fast, then the photon lightcurve (in our case the X-ray one) would track in detail the source variability. Moreover, one would expect to find a break in the PSD spectrum only for the TeV  $\gamma$ -rays, which is not the case. In fact, it is not the cooling timescale alone that determines the variability pattern of photons, but the minimum timescale between  $t_{\text{esc}}$  and  $t_{\text{cool}}$ . As is the case for all one-zone models, the fastest possible variation of the system is controlled by the photon crossing timescale  $t_{\text{cr}}$ . When  $\min(t_{\text{esc}}, t_{\text{cool}}) \approx t_{\text{cr}}$ , as in our simulations, the photon lightcurves follow, in general, the source variations. However, the small timescale variations are smoothed out. Even in the extreme case of ultra fast cooling ( $t_{\text{cool}} \ll t_{\text{cr}}$ ) photons cannot attain the full amplitude of particle variations – see Appendix B, and this results in a breaking frequency (which corresponds to a few  $t_{\text{cr}}$ ) in the PSD. Another parameter that affects the shape of the output PSD is the amplitude of the imposed variations – see parameter  $f$  in eq. (3). For some very small value of  $f$ , which in our simulations is  $f = 0.001$ , we find that the lepto-hadronic system can follow the variations at injection, i.e. the PSD of the light curves has the same shape, apart from a normalization factor, with the one of injection. However, for so small  $f$  values the variability is at a very low level, and therefore for all practical purposes the source can be considered as not varying.

For the two lepto-hadronic cases (Models LH $\pi$  and LHs in Fig. 1) we have implemented the same variation<sup>5</sup> for  $\ell_p^{\text{inj}}$ , which was further extended to  $\ell_e^{\text{inj}}$ , since two types of particles are being injected in the source. These simulations generated light curves similar to those shown in Fig. 2. More information, however, can be deduced from flux-flux diagrams, as the one shown in Fig. 3 where the TeV flux is plotted against the X-ray flux for all the cases discussed so far. First let us focus on model H (black solid line). While the X-rays follow linearly the proton synchrotron radiation, and therefore the proton luminosity, the TeV emission shows an almost quadratic dependence on  $\ell_p^{\text{inj}}$  for the reasons explained earlier – see also DMPR. Although at low fluxes one finds a clear quadratic dependence, this becomes flatter at higher fluxes due to the increasing effect of  $\gamma\gamma$  absorption

<sup>5</sup> Not only the type of variation but also the series of random numbers used in all cases is the same, unless stated otherwise.

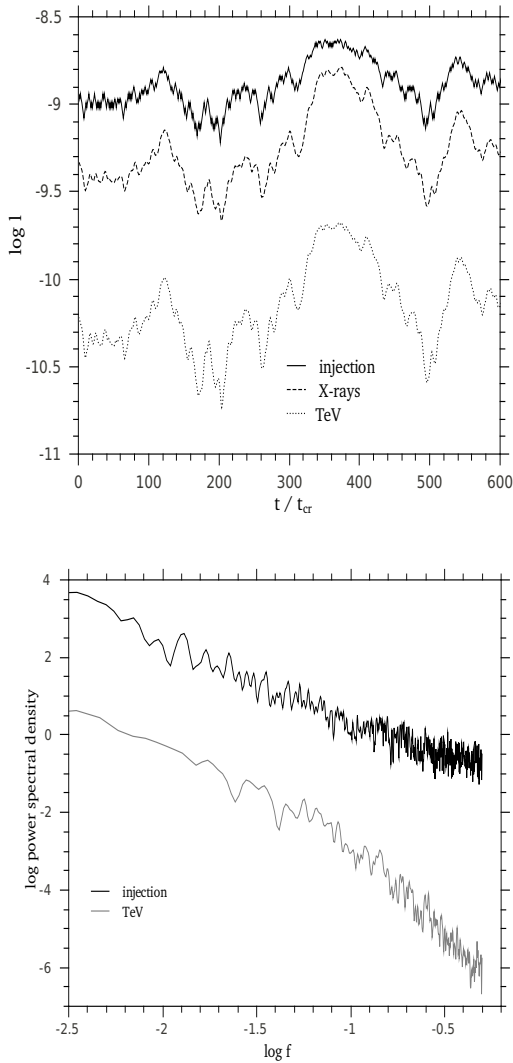


**Figure 2.** Top panel: X-ray (dashed line) and TeV (dotted line) lightcurves for the pure hadronic fit shown in Fig. 1, obtained by varying  $\ell_p^{inj}$  (thick solid line); the latter is shifted downwards by 7 units in the y-axis for clarity reasons. For the adopted parameters, one  $t_{cr}$  corresponds to  $\simeq 1.8$  hrs in the observer’s frame. Bottom panel: Power spectral density (PSD) of the injection time series (black line) and of the derived TeV light curve (grey line).

which gradually depletes the TeV regime. Another feature that is worth mentioning, is the tight correlation between the fluxes, which is derived with no requirements of fine tuning, same as in the SSC scenario.

In general, the same trend holds also for the LH $\pi$  model (dashed line), while the LHs case (grey solid line) leads to a (sub)linear correlation<sup>6</sup>. In the leptohadronic models we find no break in the TeV/X-ray correlations, since the effects of  $\gamma\gamma$  absorption are less significant. This comes from the

<sup>6</sup> A linear regression fit to the data for the LHs model gives a slope  $\sim 0.7$ ; we characterize this as a sublinear correlation. For a particular model, the exact slope of the  $F_{TeV}/F_X$  correlation depends also on the energy bands considered. For example, for the LHs model we derive an exactly linear correlation between the peak fluxes of the two distinct emission components.

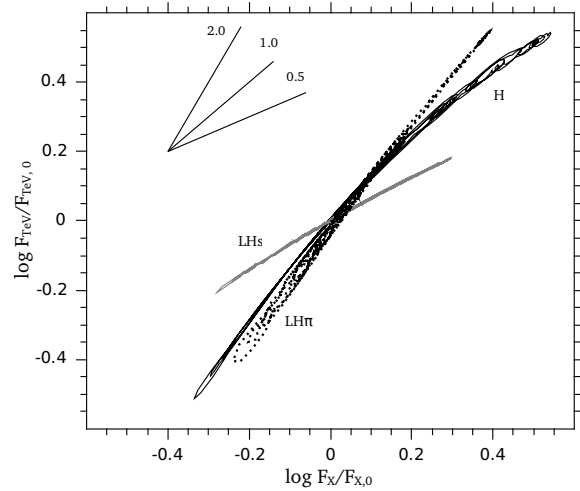


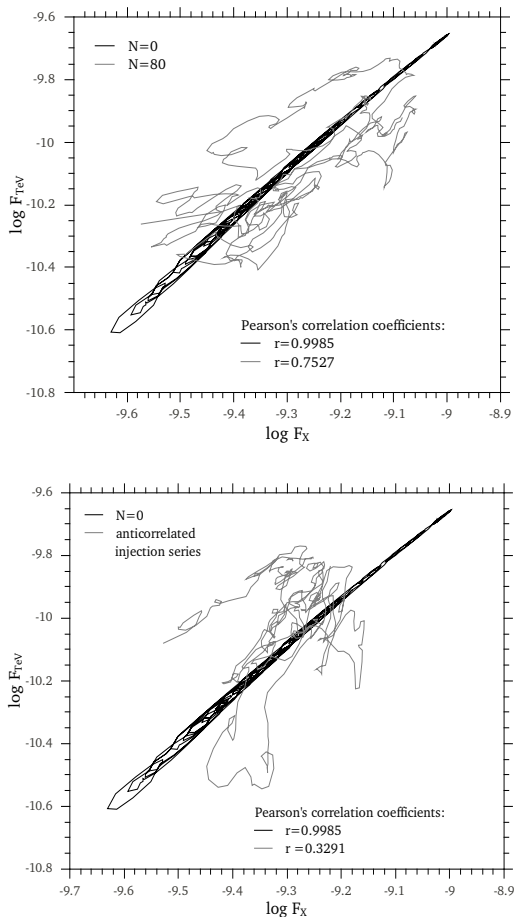
**Figure 3.** Plot of the TeV vs. X-ray fluxes obtained after varying only  $\ell_p^{inj}$  (Model H) and both  $\ell_p^{inj}$  and  $\ell_e^{inj}$  (Models LH $\pi$  & LHs). The fluxes are normalized with respect to their values of the pre-flaring state fit. Segments with different slopes are also plotted for reference.

fact that, for both models, we have obtained good fits using much smaller  $\ell_p^{inj}$  and higher Doppler factors than in the pure hadronic one – see Table 1. Finally, in all three models, no lags between the X-ray and TeV photons were detected.

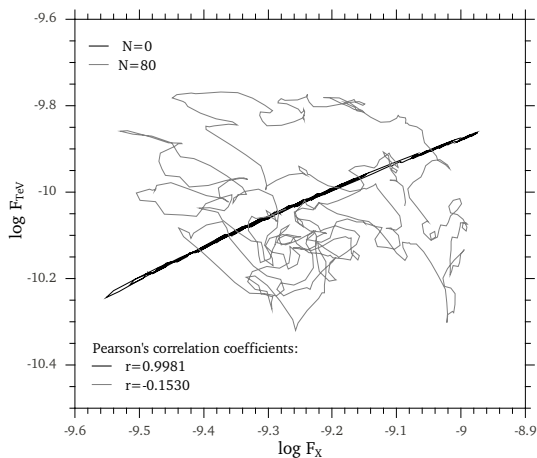
Previous analyses of Mrk 421 have noted the presence of lags in its spectral evolution (e.g. Takahashi et al. (2000); Fossati et al. (2008); Singh et al. (2012)). Such lags cannot be reproduced by one-particle population models, such as the purely hadronic one. However, in leptohadronic models where two primary particle populations are being injected into the source, these lags can be simulated by introducing a shift  $N$  in the temporal variation of  $\ell_e^{inj}$  compared to  $\ell_p^{inj}$ , i.e.  $(\ell_e^{inj})_i = (\ell_p^{inj})_{i+N}$ , where the subscript denotes that quantities are calculated at time  $t_i$  (in units of  $t_{cr}$ ).

Figure 4 depicts the TeV vs. X-ray flux obtained in the LH $\pi$  case. In both panels, the black line corresponds to  $N = 0$ , i.e.  $\ell_p^{inj}$  and  $\ell_e^{inj}$  are completely correlated. The grey line in the top panel is the result of a simulation, where  $\ell_e^{inj}$  was obtained by a relative shift of 80  $t_{cr}$  with respect to  $\ell_p^{inj}$ . In this way we imposed less correlated variations on particle injection, having a Pearson’s correlation coefficient  $r = 0.63$ . We have used a variety of positive correlated  $\ell_p^{inj}$ ,  $\ell_e^{inj}$  by introducing various shifts, e.g.  $N = 312, 512, 1024$ . In all cases, which we do not present here, we derived large correlation coefficients ( $r \gtrsim 0.5$ ) which show that the TeV and X-ray fluxes retain their strong correlation. Then, we considered a more extreme case, where the proton and electron injection have strong anticorrelation. For this, we have used two random number series with correlation coefficient  $r = -0.7$ . The resulting TeV/X-ray correlation is shown with grey line in the bottom panel. The respective diagram for the LHs model and  $N = 80$  are shown in Fig. 5.

In general, the introduction of a shift loosens the  $F_{TeV} - F_X$  correlation. The effect, however, is more evident in the proton synchrotron case where the TeV/X-ray flux correlation is almost destroyed even for  $N = 80$  ( $r = -0.15$ ). On the other hand, in the LH $\pi$  model, even if the input series are anticorrelated, we find a larger absolute value for the



**Figure 4.** Top panel: Plot of the TeV vs. X-ray fluxes obtained within the LH $\pi$  model, after varying  $\ell_p^{\text{inj}}$  and  $\ell_e^{\text{inj}}$  with  $N = 0$  (black line) and  $N = 80$  (grey line). Bottom panel: Same as above except for the grey line, which is obtained using as input for  $\ell_p^{\text{inj}}$  and  $\ell_e^{\text{inj}}$  two different anticorrelated time-series. Inset legends show the Pearson's correlation coefficients for each case.



**Figure 5.** Plot of the TeV vs. X-ray fluxes obtained within the LHs model, after varying  $\ell_p^{\text{inj}}$  and  $\ell_e^{\text{inj}}$  with  $N = 0$  (black line) and  $N = 80$  (grey line). Inset legend same as in Fig. 4.

correlation coefficient – see inset legend of Fig. 4. In other words, if the  $\gamma$ -rays are modelled by the emission of secondaries produced by photohadronic processes and therefore any variations of  $F_{\text{TeV}}$  reflect only indirectly the changes in the proton injection rate, the correlation between the fluxes in the X-rays and TeV  $\gamma$ -rays is partially retained. On the other hand, in the LHs model the variability observed in both X-rays and  $\gamma$ -rays reflects directly the variability pattern of the particle injection rate. Thus, if there is a degree of decorrelation in the injection it will be seen also in the flux-flux diagram. For the LH $\pi$  case (top panel) the introduction of a shift decreases the maximum/minimum flux values in both energy bands, since the  $\gamma$ -ray luminosity depends also on the number density of soft target photons, e.g. synchrotron photons in the X-rays. In the LHs case on the other hand, where the  $\gamma$ -rays are the product of proton synchrotron radiation, the  $\gamma$ -ray flux does not depend on the X-ray photons, as long as the X-ray photon number density is low enough as not to cause significant  $\gamma\gamma$  absorption. Thus, the range of flux variations remains approximately the same.

### 3.3 Varying $\gamma_{\text{max}}$

Observations of Mrk 421 during different periods of flaring activity indicate spectral evolution, and in particular spectral hardening in the X-rays and/or in the TeV  $\gamma$ -rays (e.g. Takahashi et al. 2000; Fossati et al. 2008). Variations of the injection compactness alone cannot reproduce these observational findings. This is exemplified in Fig. 6, where the spectral indices<sup>7</sup> in the X-ray (grey line) and TeV energy bands (black line), are plotted against the corresponding fluxes, for one of our fitting models (LH $\pi$ ). The X-ray spectral index remains approximately constant during flux variations, while the  $\gamma$ -ray part of the spectrum becomes softer during flaring events. This is to be expected, since the TeV observations were fitted by the cutoff of the synchrotron component, in all three of our models. We note also that if  $\gamma\gamma$  absorption is significant in the TeV regime, one expects to find an almost constant spectral index, even though the injection compactness varies. These two features, i.e. absence of spectral evolution in the X-rays and/or spectral softening in the  $\gamma$ -ray regime, are also obtained for the pure hadronic and the proton synchrotron case.

The second varying parameter that we have studied is the maximum energy of protons and electrons. We have kept constant the injection compactnesses and we have once again adopted the same random number series as in §3.2 for both  $\gamma_{e,\text{max}}$  and  $\gamma_{p,\text{max}}$ . In Figs. 7 and 8 we show indicatively the results for the lepto-hadronic cases. For the proton synchrotron case, the linear flux-flux correlation is retained, in contrast to the photopion case. For the latter, we find a correlation between the TeV and X-ray fluxes, which is steeper than the quadratic we have obtained by varying  $\ell_p^{\text{inj}}$  and  $\ell_e^{\text{inj}}$ . Actually, a fit to our results shows that  $F_{\text{TeV}} \propto F_X^{3.3}$ . In the LH $\pi$  model the exact slope of the TeV/X-ray flux correlation is sensitive to the power-law exponent of the electron distribution. If the power-law spectrum of electrons at injection is flat, as in our LH $\pi$  fit (see Table 1), any variations

<sup>7</sup> We define the spectral index as  $F_\nu \propto \nu^\beta$ .



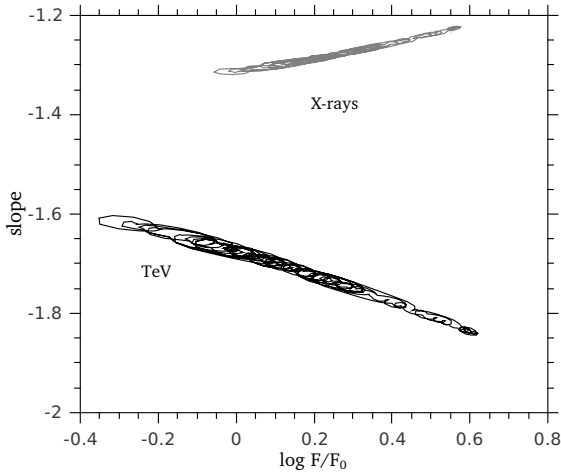


**Figure 6.** Plot of the spectral index  $\beta$  as a function of the flux in the X-rays (grey line) and in the TeV energy regime (black line) for the photopion model, in the case where the injection compactness is the varying parameter. The fluxes are normalized with respect to their values obtained for the pre-flaring fit shown in Fig. 1.

**Table 2.** Slope of the TeV/X-ray correlations obtained for variations on two model parameters.

Parameter	Model H	Model LH $\pi$	Model LHs
$\ell_{\text{inj}}$	linear to quadratic	quadratic	$\sim$ linear
$\gamma_{\text{max}}$	quadratic	quadratic to cubic	$\sim$ linear

of  $\gamma_{e,\text{max}}$  result in non-negligible variations of the injection rate, since  $\ell_{\text{e}}^{\text{inj}}$  is kept constant. Thus, the number density of synchrotron photons emitted by electrons with  $\gamma < \gamma_{e,\text{max}}$ , which serve as targets for protons, vary significantly. In such case, we expect that the  $\gamma$ -ray emission will show also large variations, since it depends on both the soft photon field and the proton distribution. On the other hand, when fitting the SED with a steeper power-law electron distribution (e.g.  $p_e = p_p = 1.5$ ), the injection rate of lower energy electrons remains approximately constant. In this case, we obtain a quadratic relation between TeV and X-ray fluxes.

Following the same procedure as in §3.2, we have then studied the effects of partially correlated variations of  $\gamma_{p,\text{max}}$  and  $\gamma_{e,\text{max}}$  on the TeV/X-ray correlation. We find that the degree of TeV/X-ray flux correlation is more easily destroyed in the LHs model. As for the LH $\pi$  model is concerned, we find, for the same shift, a more tight correlation in the case of variable injection than of variable energy cutoff.

The TeV/X-ray correlations obtained so far (for correlated input time-series) are summarized in Table 2. The symbol ‘ $\sim$ ’ is used to denote possible deviations from the exact trend due to effects that do not depend on the fitting model itself, such as  $\gamma\gamma$  absorption and the particular choice of the energy bands.

Figure 8 shows that an increasing flux in both X-rays (bottom panel) and  $\gamma$ -rays (top panel) is accompanied by

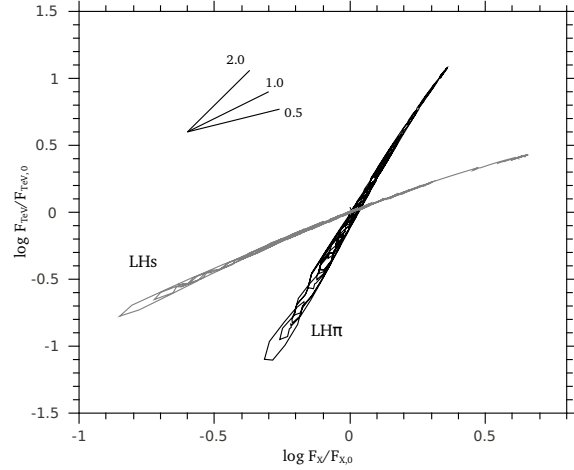


**Figure 7.** Plot of the TeV vs. X-ray fluxes obtained after varying both  $\gamma_{p,\text{max}}$  and  $\gamma_{e,\text{max}}$  in Models LH $\pi$  & LHs shown in black and grey color respectively. The fluxes are normalized with respect to their values of the pre-flaring state fit. Segments with different slopes are also plotted for reference.

a hardening of the spectrum; this trend is in good agreement with many observations regarding spectral variability of Mrk 421. Figure 8 reveals also a ‘mirror’ symmetry between the photopion and proton synchrotron cases, i.e. the range of flux and spectral variations is larger in the TeV energy band for the LH $\pi$  model and in the X-rays for the LHs. More specifically, the fact that  $\beta_X$  varies less in the photopion case than in the proton synchrotron one can be used as diagnostic tool between the two models. The range of spectral variations in the two models is better displayed in Fig. 9, where the spectral index in the TeV energy range is plotted against the one in the X-rays. Although  $\beta_{\text{TeV}}$  varies approximately between the same values in both models, spectral variations in the X-rays are more prominent in the proton synchrotron model. In particular, we find  $\beta_{\text{TeV}} \propto 3.3\beta_X$  and  $\beta_{\text{TeV}} \propto 1.1\beta_X$  for LH $\pi$  and LHs respectively.

The X-ray spectrum in the photopion case is relatively hard and shows smaller spectral variations due to the Bethe-Heitler component. If we artificially switch-off the channel of photopair production, find a fit to the pre-flaring state of Mrk 421 and then produce variations to  $\gamma_{e,\text{max}}/\gamma_{p,\text{max}}$  as before, we find that the range of variations for both  $\beta_X$  and  $F_X$  increases; specifically,  $\beta_X$  and  $\log F_X$  vary between  $(-1.7, -1)$  and  $(-9.9, -8.5)$  respectively, while their correlation law remains unaffected. Therefore, if the emission from the Bethe-Heitler process is neglected, no significant discrepancy between LH $\pi$  and LHs models is predicted.

#### 4 SUMMARY/DISCUSSION

In the present paper we have examined the spectral and variability signatures of the so-called (lepto)hadronic models. These models are routinely used to model MW observations of high energy blazars and constitute a viable alternative to the leptonic ones. According to standard practice, the low frequency part of the spectrum (usually up to the X-ray regime) is fitted by electron synchrotron radiation, while the



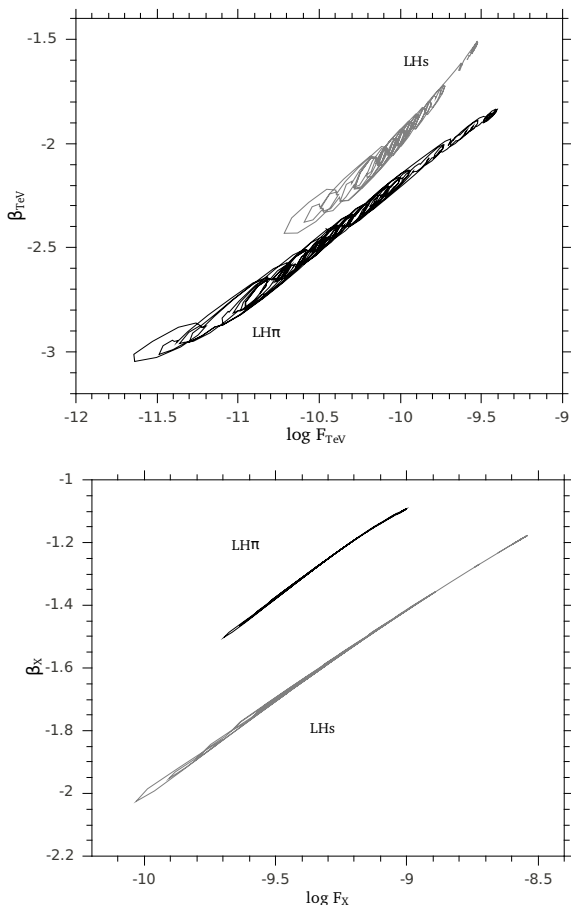


**Figure 8.** Plot of the spectral index  $\beta$  as a function of the flux  $F$  in the TeV energy band (top panel) and in the X-rays (bottom panel). Black and grey lines correspond to the  $\text{LH}\pi$  and LHs case respectively. For clarity reasons we have shifted the grey curve in the top panel by 0.2 units upwards.

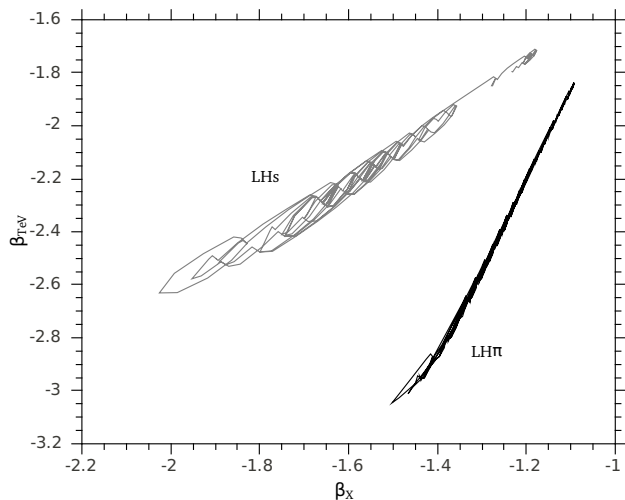


**Figure 9.** Plot of the spectral index in the TeV energy range ( $\beta_{\text{TeV}}$ ) vs. the corresponding one in the X-rays ( $\beta_X$ ) for the  $\text{LH}\pi$  (black line) and LHs (grey line) models.

higher part is fitted by hadronic emission – most commonly proton synchrotron radiation.

For the purposes of the present treatment we have used the time-dependent numerical code presented in DMPR. This models the photopair and photopion processes in great detail by using results from the Monte Carlo codes of Protheroe & Johnson (1996) and Mücke et al. (2000) respectively for the production rates of secondaries. We have chosen, as an illustrative example, to fit the well monitored TeV blazar Mrk 421 during a flaring state using the results of the 2001 campaign (Fossati et al. 2008). For this, we followed the usual algorithm (for a similar approach to the leptonic case, see Mastichiadis & Kirk (1997); Krawczynski et al. (2002)) where we first fitted the SED for a pre-flaring state and then we simulated variability by varying some key parameter of the fit – in our case it was either the particle injection luminosity or the upper cutoff of the particle distribution.

As explained in DMPR, hadronic models have three important processes which can lead to high energy photon emission. These are proton synchrotron radiation, photopair, and photopion production. In principle all three could be used, in various combinations, in attempting a fit to the SED of a  $\gamma$ -ray blazar. In practice we found that there are three combinations which give satisfactory results to the Mrk 421 case:

- (i) The ‘pure hadronic’ (H) model: In this case there is no need for a leptonic component. The X-rays are produced from proton synchrotron radiation while the TeV  $\gamma$ -rays were ‘pion induced’ – with this we mean that  $\gamma$ -rays are produced from a combination of the synchrotron radiation of electrons produced in charged pion decay and of the electromagnetic cascade induced from neutral pion decay  $\gamma$ -rays.
- (ii) The ‘lepto-hadronic pion’ ( $\text{LH}\pi$ ) model: The X-rays are produced from the synchrotron radiation of a primary leptonic component while the  $\gamma$ -rays are once again pion-induced.
- (iii) The ‘lepto-hadronic synchrotron’ (LHs) model: Here the X-rays are produced as in the previous model while the  $\gamma$ -rays are produced by proton synchrotron radiation.

All three models need high magnetic fields – as compared to the pure leptonic fits, and high values of  $\gamma_{p,\text{max}}$  with the LHs model requiring the most extreme values of both parameters. However, this is also the model that by far is the more ‘economic’ for the required energy density in relativistic protons – see Table 1.

As a next step, we introduced random-walk type perturbations either in the compactness of the injected particles or in their upper cutoff. We have assumed that each consecutive value of these parameters is either increased or decreased by 5% over its previous value. If many of these small amplitude perturbations pile up they can produce a ‘statistical’ flare and we have chosen such an example to test the variability signatures of the models listed above (see Fig. 2) – note however that nowhere does the varying parameter exceed its initial value by more than a factor of 2. Feeding the values of the varying parameter to the code we produce simulated variations in the X-ray and TeV  $\gamma$ -ray bands and searched for possible correlations between their respective fluxes and spectral indices.

In the case of a varying injection compactness, the H

model gives us a clear quadratic dependence between the X-ray and TeV  $\gamma$ -rays – this can be easily explained from the fact that the H model resembles in many aspects to the SSC leptonic one (see DMPR). An interesting feature is that at high fluxes  $\gamma\gamma$  absorption tends to linearize the correlation – see Fig. 3. The other two leptohadronic models need at least two more free parameters to fully specify their variability. One relates the amplitudes of variation between protons and electrons and the other their phases. Here we have examined the most simple cases, i.e. we have assumed equal amplitude changes between the two species which can be either contemporaneous or with a time shift of several  $t_{\text{cr}}$ . In the no-lag case, the LH $\pi$  model produces a quadratic dependence between the fluxes, while the LHs a less than linear one. Note that because of the values of the fitting parameters (see Table 1)  $\gamma\gamma$  absorption is more severe in the latter case than in the former, a fact that explains the curvature seen in the model LHs curve. In the case where we have allowed time lags, then both models loosen up their correlation. We found however that in the case of the LH $\pi$  model a general quadratic trend remains while for the LHs model all correlation is lost. Finally, all three models seem to get steeper TeV spectra as the flux increases – see Fig. 6.

In the case where the maximum energy of the particle distribution was varying, we found that the results are similar to the particle injection case, with the notable difference that all models produce a spectral hardening to both X-rays and TeV  $\gamma$ -rays. We have also found that time shifts tend to decorrelate more the lightcurves, however the effect is stronger in the LHs model than in the LH $\pi$ .

Obtaining the PSD of the light curves we find that they resemble the one of injection, up to a break frequency that corresponds to a few  $t_{\text{cr}}$ . In particular, for both TeV and X-ray light curves we find less power at the high-frequency part of their PSD (small timescale variations) when compared to that of the source. In other words, for the parameters used in the present work (see Table 1), the photon field cannot react faster than a few  $t_{\text{cr}}$  to the imposed variations – see section 3.2 and Appendix B for more details. Note also that the break frequency of the PSD corresponds to  $\sim 0.5 - 1$  days, which does not contradict other published results (e.g. Takahashi et al. (2000); Kataoka et al. (2001)).

Although we have not addressed in detail the acceleration mechanism, the adopted modelling for the variations corresponds to a physical picture, where particles first are being accelerated close to a shock front (this region is a ‘black box’ in our model) and then, they are being injected in the emitting volume. Thus, any changes that occur in the region where acceleration takes place, are later seen as changes in the characteristics of the particle injection mechanism. These on their turn lead to an outbursting behaviour of the source. Studying the characteristics of this flaring activity was the actual aim of the present work. In this respect, the introduced time-lags play the role of some intrinsic difference in the acceleration mechanism between the two species which, however, retains some coherence. Two-zone models which have been applied to leptonic models (Kirk et al. (1998) and Moraitis & Mastichiadis (2011)) are more elaborate as far as particle acceleration is concerned, however they can become very cumbersome when treating hadronic processes.

Concluding we can say that it is very interesting that

all three models give very good  $\chi^2$  fits to the Mrk 421 data – the two leptohadronic models have slightly better fits, however one should have in mind that they use many more free parameters. We note also that it is the first time that the pion-induced  $\gamma$ -ray component is used in fitting TeV data. In this case we found that a broad feature in the low to medium  $\gamma$ -rays is produced from the synchrotron radiation of Bethe-Heitler pairs (see Fig. 1). This feature is very restrictive as far as fitting is concerned, but its presence might provide a decisive observational clue for the viability of this brand of hadronic models as it is not present neither in the LHs nor in the leptonic SSC models. We also found that proton synchrotron models are favoured as far as energetics is concerned. However, we note that the H and LH $\pi$  models produce in a much more natural way correlated variability between X-rays and TeV  $\gamma$ -rays which is mostly quadratic – that is they require equal amplitude variations between the particles and can allow for shifts in their phases. Proton synchrotron models, on the other hand, are inherently linear and therefore, in order to produce quadratic correlations they need the rather special conditions that the electron injection varies quadratically with respect to the one of the protons. Furthermore, they require a tight phase correlation between the injection of the two species as all coherence is lost even in short time shifts.

The analysis presented here deals with variability signatures in the framework of leptohadronic models, such as TeV/X-ray correlation, spectral evolution in the X-rays and very high energy (VHE)  $\gamma$ -rays and PSD of the corresponding light curves. These could be used as a diagnostic tool for differentiating between the models and therefore probing the nature of high-energy radiating particles. Observational requirements for this are the high temporal and spectral resolution in the VHE part of the  $\gamma$ -ray spectrum along with contemporaneous X-ray observations. Great importance for the first requirement will be the future Cherenkov Telescope Array (CTA), since it will have high sensitivity and will provide us with large count rate light curves on a routine daily basis rather than on exceptional flaring events only (Sol et al. 2012).

## 5 ACKNOWLEDGMENTS

We would like to thank Dr. D. Emmanoulopoulos for useful discussions and comments on the manuscript. This research has been co-financed by the European Union (European Social Fund - ESF) and Greek national funds through the Operational Program “Education and Lifelong Learning” of the National Strategic Reference Framework (NSRF) - Research Funding Program: Heracleitus II. Investing in knowledge society through the European Social Fund.

## REFERENCES

- Abdo A. A. et al., 2011, *ApJ*, 736, 131
- Aharonian F. A., 2000, *New Astron.*, 5, 377
- Boettcher M., 2012, *ArXiv e-prints*
- Boettcher M., Dermer C. D., 1998, *ApJ*, 501, L51
- Dermer C. D., Schlickeiser R., 1993, *ApJ*, 416, 458

- Dermer C. D., Schlickeiser R., Mastichiadis A., 1992, A&A, 256, L27
- Dimitrakoudis S., Mastichiadis A., Protheroe R. J., Reimer A., 2012, A&A, 546, A120
- Emmanoulopoulos D., McHardy I. M., Uttley P., 2010, MNRAS, 404, 931
- Fossati G. et al., 2008, ApJ, 677, 906
- Fossati G., Maraschi L., Celotti A., Comastri A., Ghisellini G., 1998, MNRAS, 299, 433
- Ghisellini G., Madau P., 1996, MNRAS, 280, 67
- Kataoka J. et al., 2001, ApJ, 560, 659
- Kirk J. G., Mastichiadis A., 1992, Nature, 360, 135
- Kirk J. G., Rieger F. M., Mastichiadis A., 1998, A&A, 333, 452
- Konopelko A., Mastichiadis A., Kirk J., de Jager O. C., Stecker F. W., 2003, ApJ, 597, 851
- Krawczynski H., Coppi P. S., Aharonian F., 2002, MNRAS, 336, 721
- Mannheim K., Biermann P. L., 1992, A&A, 253, L21
- Maraschi L., Ghisellini G., Celotti A., 1992, ApJ, 397, L5
- Mastichiadis A., Kazanas D., 2006, ApJ, 645, 416
- Mastichiadis A., Kazanas D., 2009, ApJ, 694, L54
- Mastichiadis A., Kirk J. G., 1997, A&A, 320, 19
- Moraitis K., Mastichiadis A., 2011, A&A, 525, A40
- Mücke A., Engel R., Rachen J. P., Protheroe R. J., Stanev T., 2000, Computer Physics Communications, 124, 290
- Mücke A., Protheroe R. J., Engel R., Rachen J. P., Stanev T., 2003, Astroparticle Physics, 18, 593
- Petropoulou M., Mastichiadis A., 2011, A&A, 532, A11
- Petropoulou M., Mastichiadis A., 2012a, MNRAS, 426, 462
- Petropoulou M., Mastichiadis A., 2012b, MNRAS, 421, 2325
- Protheroe R. J., Johnson P. A., 1996, Astroparticle Physics, 4, 253
- Raiteri C. M. et al., 2012, A&A, 545, A48
- Sikora M., Begelman M. C., Rees M. J., 1994, ApJ, 421, 153
- Singh K. K., Bhattacharyya S., Bhatt N., Tickoo A. K., 2012, New Astron., 17, 679
- Sol H. et al., 2012, Astroparticle Physics
- Stawarz L., Kirk J. G., 2007, ApJ, 661, L17
- Takahashi T. et al., 2000, ApJ, 542, L105
- Ulrich M.-H., Maraschi L., Urry C. M., 1997, ARA&A, 35, 445

## APPENDIX A: LATENT PRIMARY LEPTONIC COMPONENT IN THE ‘H’ MODEL

One of the models studied in the present work is the pure hadronic (‘H’), where the two main emission components of the MW spectrum are attributed to protons. This assumption does not exclude the presence of a primary leptonic component, as long as its contribution to the total synchrotron emission in the X-ray regime is negligible.

Thus, let us derive an approximate upper limit for the injection compactness of primary electrons  $\ell_e^{\text{inj}}$ . The proton synchrotron radiated power can be calculated by

$$L_p^{\text{syn}} = \int_{\gamma_{\text{p,min}}}^{\gamma_{\text{p,max}}} d\gamma n_p(\gamma) \frac{dE}{dt} \bigg|_{\text{p,rad}}, \quad (\text{A1})$$

where

$$\frac{dE}{dt} \bigg|_{\text{p,rad}} = \frac{4}{3} \sigma_T c u_B \left( \frac{m_e}{m_p} \right)^2 \gamma^2. \quad (\text{A2})$$

Assuming that protons at the injection have a power-law distribution,  $n_p = K_p \gamma^{-p}$  between  $\gamma_{\text{p,min}}$  and  $\gamma_{\text{p,max}}$ , with  $\gamma_{\text{p,min}} \ll \gamma_{\text{p,max}}$  and  $p < 3$ , the integral above results in

$$L_p^{\text{syn}} \approx \frac{4}{3} \sigma_T c u_B K_p \left( \frac{m_e}{m_p} \right)^2 \frac{\gamma_{\text{p,max}}^{3-p}}{3-p}. \quad (\text{A3})$$

The normalization constant  $K_p$  can be expressed in terms of the proton injection compactness – see eq. (1) in §2. In the case where proton cooling is not significant, the proton injection luminosity is approximately given by

$$L_p^{\text{inj}} \approx \frac{m_p c^2}{t_{\text{p,esc}}} \int_{\gamma_{\text{p,min}}}^{\gamma_{\text{p,max}}} d\gamma \gamma n_p(\gamma) \approx \frac{m_p c^2}{t_{\text{cr}}} K_p F_p, \quad (\text{A4})$$

where

$$F_p = \frac{\gamma_{\text{p,max}}^{2-p} - \gamma_{\text{p,min}}^{2-p}}{2-p} \approx \frac{\gamma_{\text{p,max}}^{2-p}}{2-p}, \text{ if } p < 2. \quad (\text{A5})$$

Thus,  $K_p$  is written as

$$K_p = \frac{4\pi R^2 \ell_p^{\text{inj}}}{\sigma_T F_p}. \quad (\text{A6})$$

For the electron distribution, on the other hand, we assume that all the injected power is radiated, i.e.  $L_e^{\text{syn}} \approx L_e^{\text{inj}}$ . Thus, the ratio of the observed X-ray luminosities of the two populations is approximately given by

$$\frac{L_e^{\text{obs}}}{L_p^{\text{obs}}} \approx \frac{L_e^{\text{syn}}}{L_p^{\text{syn}}} \approx 40 \frac{\ell_e^{\text{inj}}}{\ell_p^{\text{inj}}} \frac{3-p}{2-p} \left( \frac{\gamma_{\text{p,max}}}{10^6} \frac{R}{10^{15}} \frac{u_B}{10^2} \right)^{-1}. \quad (\text{A7})$$

Assuming that  $\frac{L_e^{\text{obs}}}{L_p^{\text{obs}}} = \chi \sim 0.1$ , the above equation gives a rough estimation for  $\ell_e^{\text{inj}}$ , which ensures that the emission features of primary electrons in the X-rays will be ‘hidden’ from the proton synchrotron component:

$$\ell_e^{\text{inj}} \approx (2.5 \times 10^{-5}) \frac{2-p}{3-p} \frac{\chi}{10^{-1}} \frac{\ell_p^{\text{inj}}}{10^{-2}} \frac{\gamma_{\text{p,max}}}{10^6} \frac{R}{10^{15}} \frac{u_B}{10^2}. \quad (\text{A8})$$

For the exact values listed in Table 1 we find  $\ell_e^{\text{inj}} \sim 4 \times 10^{-5}$ .

## APPENDIX B: SIMPLIFIED MODEL FOR THE SYSTEM’S RESPONSE TO VARIATIONS OF THE SOURCE

One of the factors that determines the response of a particle/radiation system to the variations of the source is the relation between the variability timescale of the source, which in our simulations was taken equal to  $1t_{\text{cr}}$ , and the minimum of the cooling and escape timescales of particles.

Here we show through a simplified model, that even in the non-physical case of sub-dynamical cooling of particles, i.e.  $t_{\text{cool}} \ll t_{\text{cr}}$ , the photon distribution cannot track exactly the variations of the source. For simplicity, we study the evolution of electrons and photons only. Let us assume that electrons, with number density  $n$ , are being injected into a volume with rate  $Q$  and escape in a typical timescale  $t_{\text{e,esc}}$ , while their characteristic cooling timescale is  $t_{\text{e,cool}}$ ; energy losses of electrons are treated as catastrophic. Photons, on the other hand, are escaping within  $t_{\text{cr}}$  and are

being injected with a rate  $\propto n/t_{e,\text{cool}}$ . Thus, the system is described by

$$\frac{dn}{d\tau} + n(\alpha + \chi) = Q(\tau) \quad (\text{B1})$$

$$\frac{dn_\gamma}{d\tau} + n = J\chi n, \quad (\text{B2})$$

where  $\tau = t/t_{\text{cr}}$ ,  $\alpha = t_{\text{cr}}/t_{e,\text{esc}}$ ,  $\chi = t_{\text{cr}}/t_{e,\text{cool}}$  and  $J$  is normalization constant. We model the electron injection function as a series of pulses with constant duration ( $\delta t = 1t_{\text{cr}}$ ) and variable amplitude:

$$Q(\tau) = \sum_{i=1,3,5}^N Q_{i-1} H(\tau - \tau_{i-1}) H(\tau_i - \tau), \quad (\text{B3})$$

where  $H(x)$  is the step function and

$$Q_j = Q_{j-2} + r, \quad Q_0 = 2 \text{ and } j = 2, 4, 6, \dots \quad (\text{B4})$$

and  $r$  is a uniformly distributed random number in the range  $[-3, 2]$  while  $\tau_i = \tau_{i-1} + \delta\tau$  and  $\tau_0 = 0$ . For initial conditions  $n(0) = n_\gamma(0) = 0$ , the solution for electrons and photons is given by:

*Electrons:*

$$n = f_{i-1}(\tau) \begin{cases} n(\tau_{i-1}) + \frac{Q_{i-1}}{\alpha + \chi} \frac{1 - f_{i-1}(\tau)}{f_{i-1}(\tau)}, & i = 1, 3, \dots \\ n(\tau_{i-1}), & i = 2, 4, \dots \end{cases} \quad (\text{B5})$$

where

$$f_{i-1}(\tau) = e^{(\alpha + \chi)(\tau_{i-1} - \tau)} \quad (\text{B6})$$

and each branch is valid in the time interval  $[\tau_{i-1}, \tau_i]$ .

*Photons:*

$$n_\gamma = n_\gamma(\tau_{i-1}) E_{i-1}(\tau) + J\chi \frac{Q_{i-1}}{\alpha + \chi} (1 - E_{i-1}(\tau)) + J\chi G_{i-1}(\tau) \left( n(\tau_{i-1}) - \frac{Q_{i-1}}{\alpha + \chi} \right), \quad i=1,3,5,\dots \quad (\text{B7})$$

where

$$G_{i-1}(\tau) \equiv \frac{(E_{i-1}(\tau))^{\alpha + \chi} - E_{i-1}(\tau)}{1 - \alpha - \chi} \quad \text{and} \quad (\text{B8})$$

$$E_{i-1}(\tau) \equiv e^{\tau_{i-1} - \tau}. \quad (\text{B9})$$

The solution for  $i = 2, 4, 6$  is given below

$$n_\gamma = n_\gamma(\tau_{i-1}) E_{i-1}(\tau) + J\chi \frac{n(\tau_{i-1})}{1 - \alpha - \chi} \cdot [(E_{i-1}(\tau))^{\alpha + \chi} - E_{i-1}(\tau)]. \quad (\text{B10})$$

Figure B1 shows the time-evolution of photons for three cases: (i) sub-dynamical cooling and fast particle escape with  $\chi = 100, \alpha = 1$  (top panel), (ii) slow cooling and fast escape with  $\chi = 0.1, \alpha = 1$  (middle panel) and (iii) slow cooling and escape with  $\chi = 0.1, \alpha = 0.1$  (bottom panel). The normalization constant in examples (i)-(iii) was chosen to be  $J = 1, 20, 5$  respectively. Note that even in the extreme case of ultra fast cooling (top panel) the photon lightcurve does not have exactly the shape of the injection pulses. Thus, the power spectral density (PSD) of the injection and photon time series will differ below some frequency  $f_{\text{br}}$ . This effect will be even more prominent in examples (ii) and (iii), since

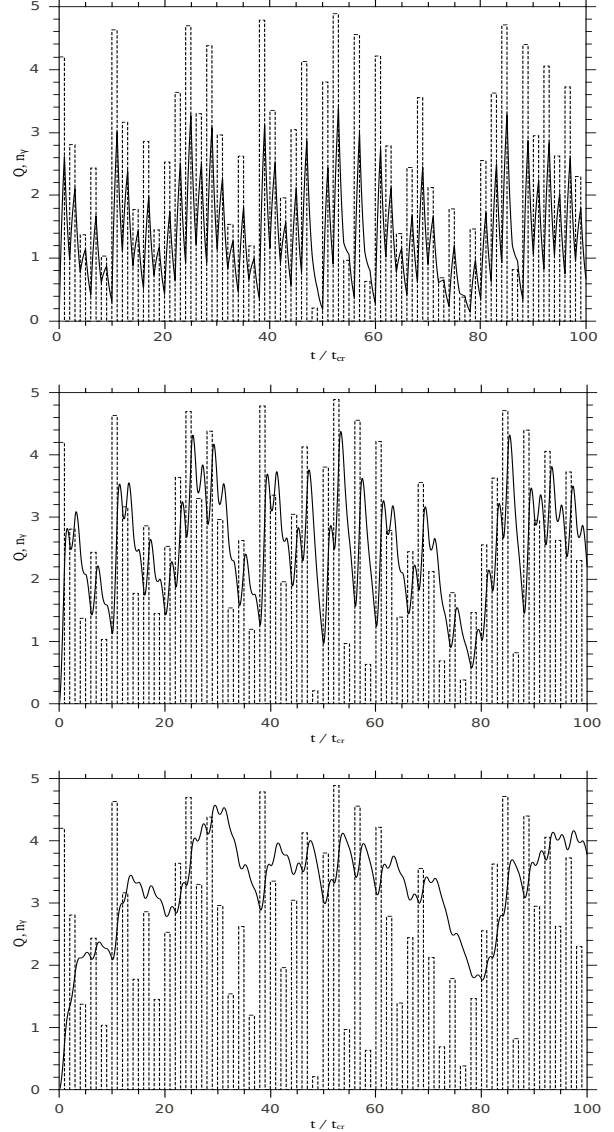


**Figure B1.** Response of the photon distribution to the variations of electron injection for:  $\chi = 100, \alpha = 1$  (top panel),  $\chi = 0.1, \alpha = 1$  (middle panel) and  $\chi = 0.1, \alpha = 0.1$  (bottom panel). The injection function is depicted with dashed lines in all cases.

the photon lightcurve becomes smoother and loses the details in small timescales – see middle and bottom panels in Fig. B1. In general, the temporal behaviour of the system including all physical processes, is satisfactorily described by one of the categories of the simplified model:

- Fast cooling and escape, i.e.  $t_{\text{cool}} \lesssim t_{\text{esc}} = t_{\text{cr}}$ . The leptonic component of our models belongs to this category, that corresponds to case (i) – top panel in Fig. B1.
- Slow cooling and fast escape, i.e.  $t_{\text{cool}} \gg t_{\text{esc}} = t_{\text{cr}}$ , which characterize the proton distribution in all our three models. Only in the LHs model, protons at the high-energy tail of the distribution have cooling timescales comparable to  $t_{\text{cr}}$ . This category corresponds to case (ii) – middle panel in Fig. B1.
- Slow cooling and escape, i.e.  $t_{\text{cool}} \approx t_{\text{esc}} \gg t_{\text{cr}}$ . For the

fitting parameters adopted in the present work, neither the proton nor the leptonic distribution falls into this category, which corresponds to case (iii) – bottom panel in Fig. B1.